PROCEEDINGS OF SCIENCE

Status and Performance of the Underground Muon Detector of the Pierre Auger Observatory

Joaquín de Jesús [a,b,*] **for the Pierre Auger Collaboration**[c]

[a] *Instituto de Tecnología y Detección en Astropartículas (CNEA, CONICET, UNSAM), Buenos Aires, Argentina*

[b] *Karlsruhe Institute of Technolgy (KIT), Institute for Astroparticle Physics, Karlsruhe, Germany*

[c] *Observatorio Pierre Auger, Av. San Martín Norte 304, 5613 Malargüe, Argentina*

Full author list: https://www.auger.org/archive/authors_icrc_2023.html

E-mail: spokespersons@auger.org

The Pierre Auger Observatory, located in Malargüe, Argentina, is the largest facility for the detection of ultra-high-energy cosmic rays and has been operating successfully for nearly 20 years. For its second phase of operation, the Observatory is undergoing a major upgrade, called AugerPrime, to increase its sensitivity to the primary mass. As part of the upgrade, the Underground Muon Detector is being deployed in the low-energy extension of the Surface Detector. It consists of an array of 30 m^2 plastic scintillator muon counters buried 2.3 m underground in the vicinity of the water-Cherenkov detectors. This will allow a direct measurement of the muonic component of air showers in the energy range $10^{16.5}$ eV to 10^{19} eV, contributing significantly to the discrimination of the primary mass and to the testing of hadronic interaction models. In this contribution, the deployment status and performance of the Underground Muon Detector are presented.

The 38th International Cosmic Ray Conference (ICRC2023)
26 July – 3 August, 2023
Nagoya, Japan

*Speaker

PoS(ICRC2023)267

1. Introduction

The Surface Detector (SD) [1] of the Pierre Auger Observatory is comprised of an array of 1660 water-Cherenkov detectors (WCD) ordered in three nested triangular grids with spacing of 1500 m (SD-1500), 750 m (SD-750) and 433 m (SD-433). The SD-1500 covers an area of 3000 km^2 and provides an energy threshold of $10^{18.5}$ eV whereas the SD-750 comprises an area of 23.5 km^2 with an energy threshold of $10^{17.5}$ eV. Finally, the SD-433 encloses a smaller area of 1.9 km^2 and is suitable for energies above $10^{16.5}$ eV.

Currently, the Observatory is undergoing an upgrade known as AugerPrime [2] involving several enhancements: (i) the addition of a small photomultiplier tube to the WCDs in order to expand their dynamic range; (ii) the installation of a plastic scintillator, the Surface Scintillator Detector (SSD), on top of the WCDs to provide an additional and complementary measurement of the particles in the shower; (iii) a Radio Detector (RD), consisting of a radio antenna placed on top of the WCDs, aims to measure the radio signals produced during the development of the shower; (iv) an Underground Muon Detector (UMD), which is the focus of this contribution; and (v) the replacement of the original electronic boards of the SD stations with new upgraded boards with faster sampling rate and increased dynamic range, also enabling communication between the SD and the SSD, RD and UMD.

2. Underground Muon Detector

The Underground Muon Detector (UMD) is being deployed in the SD-750 and SD-433 arrays. It consists of an array of plastic scintillator muon counters, each of which is buried beneath 2.3 m in the vicinity of an SD station. The soil above each detector is responsible for absorbing the electromagnetic component of air showers, and imposes an energy cut of $\sim$1 GeV for vertical muons. Each UMD station comprises three modules of 10 m^2 of plastic scintillator. In turn, a module is segmented into 64 strips of 400 cm long, 4 cm width and 1 cm thickness, with embedded wavelength-shifting optical fibers coupled to an array of 64 silicon photomultipliers (SiPM).

To increase its dynamic range, two complementary modes of operation are implemented in the UMD modules: the binary and the analog-to-digital converter (ADC) mode. The binary mode, designed for sampling low muon densities, relies on the segmentation of the detector and handles each of the 64 SiPM signals independently. The output of each SiPM is processed by a dedicated channel, comprised by a pre-amplifier, a fast shaper and a discriminator, in one of two 32-channels Application-Specific Integrated Circuit (ASIC). The output signal of the discriminator is sampled by an Field-Programmable Gate Array (FPGA) at 320 MHz (3.125 ns sample time). This leads to a binary trace (i.e. composed by 0s and 1s) of 2048 samples per SiPM. In each sample, a "1" or "0" is output if the fast shaper signal was above or below the discriminator threshold, respectively. An offline strategy is subsequently used to convert raw binary traces into number of muons: any pattern of four or more consecutive 1s in the binary trace is considered to be produced by a muon and is referred to as single-muon pattern [3]. On the other hand, the ADC mode, designed for high muon densities, treats the module as a whole as it does not depend on detector segmentation. In this mode, the 64 SiPM signals are summed and subsequently amplified with a high- and a low-gain amplifier. The amplified signals are digitized with two ADCs with a sampling time of 6.25 ns giving rise to

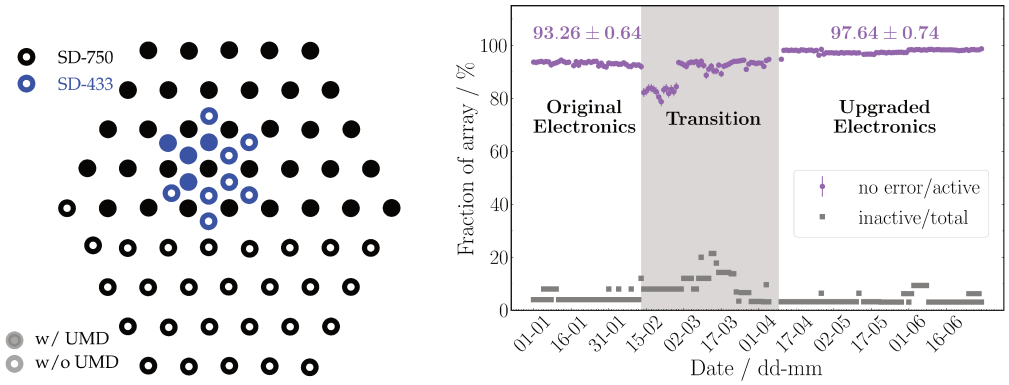

Figure 1: *Left:* Layout of the UMD array and its current deployment status. *Right:* Success rate of the UMD array between January and June 2023. The grey dashed area corresponds to the period in which the original electronics were replaced by the upgraded electronics in the SD-750 and SD-433 arrays. Grey data points show the fraction of inactive modules.

two wave forms of 1024 samples. The number of muons is obtained dividing the charge of these signals by the mean charge of a single muon.

3. Deployment status and operations

Currently, there are 52% of the UMD positions deployed as shown in the left panel of Fig. 1. At the current production and deployment rate it is foreseen to have the array fully deployed by June 2024.

The UMD relies on external triggers from the SD to operate, which are organized in a hierarchical way. The Central Data Acquisition System (CDAS) of the Observatory constantly receives time stamps of local station triggers coming from the WCDs [4], and it scans for air-shower events by requiring spatial and temporal correlations between them. If such correlations are found, it generates an event trigger to the participating stations and adjacent ones. These stations then respond by transmitting their event data.

When a local trigger is generated in an SD station, a signal is sent to the electronics of its associated UMD modules to save its data in its internal memory. When an event trigger arrives, the SD station sends another signal to the UMD modules requiring for its data. If the data is found in its circular buffer, then it is sent to the CDAS. If it is not, the UMD module's electronics responds with an error message indicating that data was lost. It is therefore of utmost importance to monitor the absence of error messages in the UMD electronics to ensure a proper operation of the detector.

To this end, a daily success rate can be defined for each module as the fraction of times in which the electronic responded without any error message upon an event trigger request. A success rate at the array level is then defined as the average success rate of all the active UMD modules. Active modules are those that are actually in acquisition from which a response is expected (either an error message or not). Inactive modules are detectors that are deployed but not in acquisition, shown as grey data points in the right panel of Fig. 1. On the same panel, the daily array success rate is shown from January to June 2023 as magenta markers. A fairly constant rate of 93% can be found up to mid February, when the installation campaign of the new electronics in the stations of the SD-750

and SD-433 arrays started. This transition period lasted until the first week of April, after which a stabilization of the rate is achieved around 97%. Therefore, an increase in the detector success rate is achieved with the new electronics. This result is expected since with the original electronics, an auxiliary board was needed for the signal transmission between the SD station and its UMD modules [5]. This added an extra step in the communication process, increasing the likelihood of errors or data loss. All the functionalities of this auxiliary board are now included in the upgraded electronics.

4. Detector characterization

Fiber attenuation plays a major role in signal fluctuations as a muon hitting the closest to the SiPM can yield almost twice the number of photon-equivalents than one hitting the furthest. This translates into having a larger number of 1s (charge) in the binary (ADC) trace when muons hit the strip closer to the SiPM. This effect was characterized under controlled conditions in the laboratory [6].

A study like that conducted in the laboratory is not feasible with deployed modules as the impact point of the muon in the strip is unknown during an air-shower event. However, the attenuation of photons in the fiber can be assessed using the fact that strips in the UMD modules have different fiber lengths. Since the dome with the SiPM array is in the center of the detector, the length of the fiber between the end of a strip and the SiPM array, referred to as manifold length, is different for each strip (see inset in left panel of Fig. 2). Due to the symmetry of the module, this leads to 16 groups each composed by 4 strips with the same fiber length. Consequently, we expect both the mean number of 1s and charge produced by a single muon to be lower in strips with longer fibers.

To inspect for a fiber effect in data, the average number of 1s, $\langle$#1s$\rangle$, in all the strips of every module was obtained using three years of air-shower events. Then, the mean value of $\langle$#1s$\rangle$ of all the strips sharing the same manifold length was determined. The result is shown in the left panel of Fig. 2. The fiber effect is quite clear as there is an anti-correlation between the manifold length and $\langle$#1s$\rangle$, which translates into a difference of ∼5% in the number of 1s between the shortest and longest fiber.

The fiber effect was additionally studied with the ADC channel following a similar procedure. For this purpose, modules with only a single strip with a single muon pattern in its binary trace were selected to guarantee that only one muon hits the detector. Subsequently, the ADC trace was integrated to obtain its charge. The set of single-muon ADC traces and the resulting charge histogram for a selected module is shown in the left panel of Fig. 3, where $t_{\max}$ denotes the time in which the ADC traces reaches its maximum. The mean value of all the strips sharing the same manifold length was obtained, as displayed in the right panel of Fig. 2. Like in the binary channel, the fiber attenuation is quite clear as strips with longer fibers have lower single-muon charge values which yields a difference of ∼15% between the shortest and the longest fiber. This confirms and validates the expected behaviour of the detector and provides an estimate of the fiber effect to be accounted for in any subsequent high-level physics analysis.

In the right panel of Fig. 3, single-muon charge as function of the secant of the shower zenith angle $\sec\theta$ is displayed for data (unfilled green markers) and simulations (filled black markers). A discrete library using proton as primary with energy $\lg(E/\mathrm{eV}) = 17.5$, zenith angles

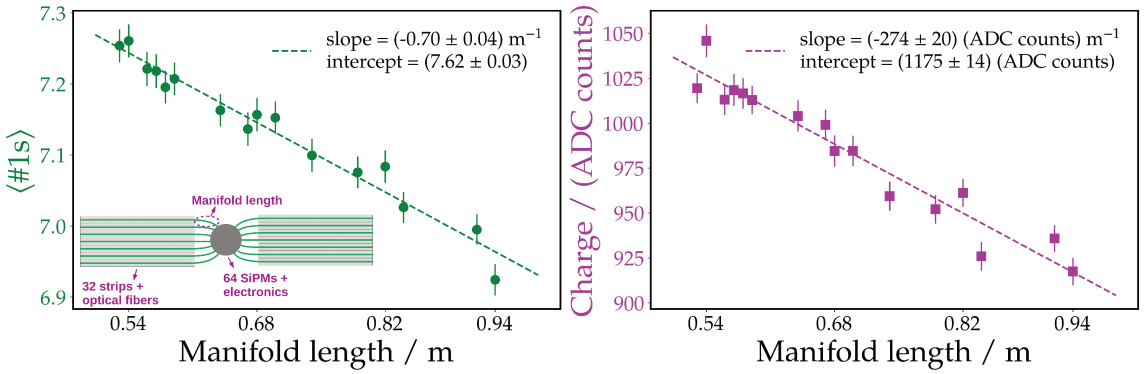

Figure 2: Mean number of 1s in the binary trace (left) and mean single-muon charge (right) as function of manifold length. As a consequence of fiber attenuation, signals decrease as the fiber length increase. The inset in the left panel shows a sketch of a UMD module indicating the manifold length.

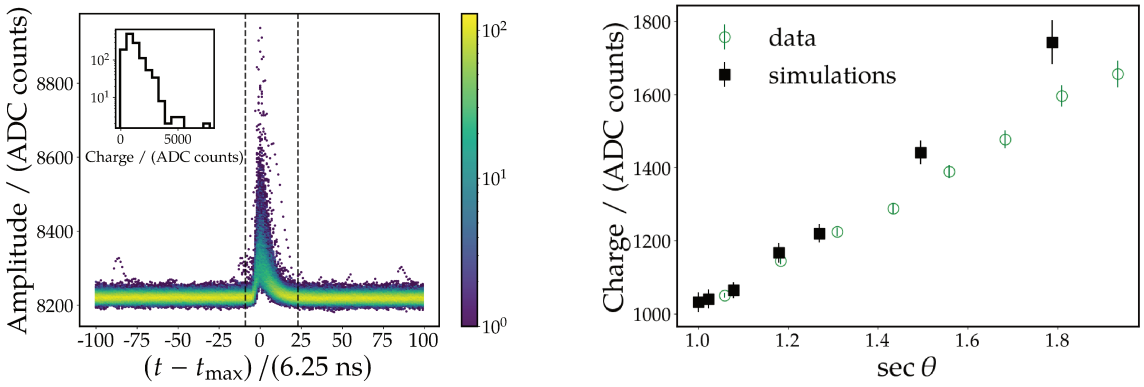

Figure 3: *Left:* Single-muon ADC traces of a selected module in air shower events. Vertical dashed lines correspond to the integration window. The inset plot displays the corresponding charge histogram. t_{max} is the time in which the ADC trace reaches its maximum. *Right:* Angular dependence of the single-muon charge. The measurements of all the modules were used scaling the charge values to a reference module as explained in Section 5.

$\theta/^\circ = \{0, 12, 22, 32, 38, 48, 56\}$ and EPOS-LHC as the hadronic interaction model was used. Data from all the modules were used by scaling to a reference module as explained in Section 5. It is apparent that single-muon charge increases for more inclined showers. This is expected due to increasing muon track length in the detector. However, it is clear that data and simulations have different slopes. Further investigation is needed to understand the origin of this discrepancy.

5. Long-term behaviour

Since the environmental conditions, such as temperature, in which the detector operates cannot be controlled, it is crucial to monitor the long-term behaviour of the signals. This is necessary to account for any seasonal effect in any subsequent higher-level physics analysis.

For every local station trigger, an algorithm running in parallel to acquisition scans over the 64 binary traces; if only one muon pattern is found in the whole module, the charge of the ADC trace

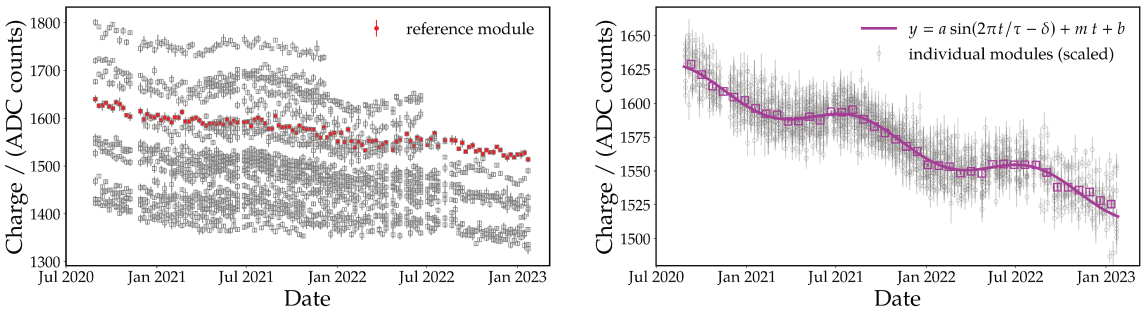

Figure 4: *Left:* Raw time series of the online single-muon charge estimate. Some modules have not measurements during the whole period due to malfunctioning or bad data taking periods. Module-to-module variations can be seen due to SiPM gain differences between the modules. Red markers show the time series of the reference module to which all the modules are scaled. *Right:* Scaled time series. Unfilled magenta markers shows the profile over the whole set of modules. The magenta line corresponds to the fit of a sinus (seasonal fluctuations) plus a linear term (aging).

is computed and streamed [3]. We will refer to the single-muon charge estimated this way as *online* charge. In the left panel of Fig. 4, the weekly mean of the online charge is shown for a set of modules deployed over 2019, for which enough data is available for a long-term analysis. Module-to-module differences can be observed due to different SiPM gains between the modules. Thus, the time serie of an arbitrary module was chosen as a reference (red markers in left panel of Fig. 4) and a scaling factor for each module was fitted to match this reference. The result of this is displayed on the right panel of Fig. 4. It is evident that a universal behaviour arises which includes a seasonal fluctuation and a long-term drift related to the aging of the detector. In a phenomenological approach, we fit a model that incorporated a sinusoidal component to capture the seasonal oscillations, along with a linear component to represent the aging effect. The fluctuations correspond to $\pm 1\%$ whereas the aging rate (slope of the linear term) is of $-2.5\%/\mathrm{yr}$.

The biweekly mean of the #1s using air-shower events was obtained for each module in the same time period. The raw time series are shown in the left panel of Fig. 5. The same module as previously chosen was selected as a reference for scaling the remaining modules. The scaled time series along with the profile over all the detectors and a fit to the same model is shown in the right panel of Fig. 5. The same qualitative behaviour seen in Fig. 4 is found. In this case, a seasonal fluctuation of $\pm 1\%$ along with an aging rate of $-0.7\%/\mathrm{yr}$ is observed. The difference in aging rate between the ADC and binary modes can be attributed to the fact that the ADC mode is sensitive to the signal charge, whereas the binary mode relies on an amplitude threshold, thus being sensitive to the signal amplitude.

In addition, the long-term behaviour of the SiPM gains was assessed. It is known that the SiPM gain decreases with temperature. For that reason, a temperature compensation mechanism is implemented in the high-voltage source of the electronics [3]. Still, there may be some minor residual temperature dependence remaining. It is thus important to verify that this residual dependence remains within acceptable limits. Measurements of the SiPM gain were periodically performed for over a year in a single module following the procedure detailed in Ref. [8]. The gain for each SiPM was determined in each measurement and the average value over the 64 channels was obtained. The

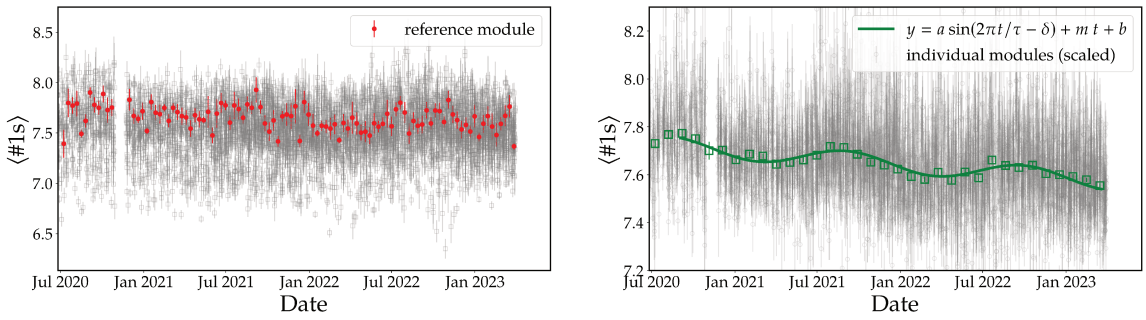

Figure 5: *Left:* Raw time series of the #1s for each module. Module-to-module variations can be seen due to gain fluctuations between the modules. Red markers show the time series of the reference module to which all the modules are scaled. *Right:* Scaled time series. Unfilled green markers shows the profile over the whole set of modules. The green line corresponds to the fit of a sinus (seasonal fluctuations) plus linear term (aging).

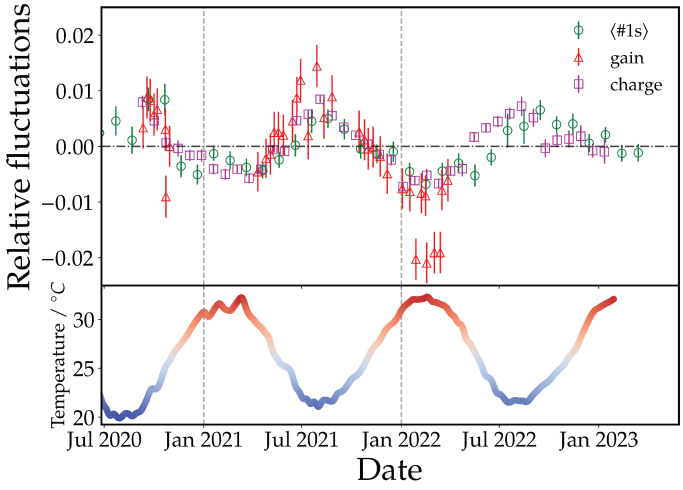

Figure 6: Magenta (green) markers represent the relative fluctuations of the charge in the ADC trace (⟨#1s⟩ in the binary trace) after the linear term associated with aging was subtracted. Red markers show the relative fluctuations of the SiPM gain, obtained as the average gain over all the 64 SiPMs for each measurement. The lower plot displays the average temperature registered by a sensor located in the UMD electronics. Grey dashed vertical lines enclose one year period.

relative fluctuations of the average gain is shown in red markers in Fig. 6. A fluctuation of ±1% is observed, being as expected larger for lower temperatures. This level of fluctuation in the gain is negligible and has no impact on the detector performance. It is however useful to explain the oscillations observed in the binary and ADC signals. For this, the linear term of the model that was fit to the time evolution of the online charge and ⟨#1s⟩ (right panel of Fig. 4 and Fig. 5) was subtracted from the data points. The relative fluctuations of these aging-corrected quantities are also shown in Fig. 6. It is apparent that the seasonal modulation in the signals are highly consistent with that found in the gain.

As already mentioned, the online charge estimate requires two conditions: a local trigger from the SD station and a single-muon pattern in the whole module. These two conditions are fulfilled

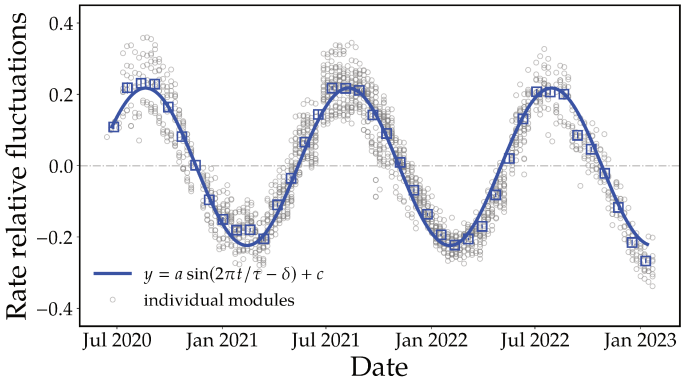

Figure 7: Relative fluctuations in the rate of the signals compatible with a single muon used for the online estimate of the single-muon charge.

with an average rate of ~ 0.1 Hz with a clear seasonal modulation, as shown in Fig. 7. This has been already reported in Ref. [7] using a shorter period of time. This oscillation is now confirmed and is found to be within a range of $\pm 20\%$. Therefore, it cannot be explained by the $\pm 1\%$ modulation in the SiPM gain. The comprehension of this effect exceeds the scope of this contribution and is currently under study.

6. Summary

The current status of the Underground Muon Detector of the Pierre Auger Observatory was presented. Firstly, an improvement in the success rate of the UMD electronics was achieved through the new upgraded electronic boards in the SD. In addition, fiber attenuation was characterized both in binary and ADC mode using field data, validating the expected behavior of the detector. Finally, the long-term behaviour of the signals was studied and an aging effect along with a seasonal fluctuation of $\pm 1\%$ was found, the latter being consistent with SiPM gain fluctuations. The discrepancy between data and simulations in the evolution of the single-muon charge with the zenith angle and the strong seasonal fluctuation in the rate of the online charge are presently undergoing investigation.

More than half of the UMD array is already deployed and fully functional, which will provide a highly valuable data set of the muon content in extensive air showers. This analysis provides a step forward towards the validation and understanding of the detector performance, which is critical for any subsequent physics analysis.

References

[1] The Pierre Auger Collaboration, Nucl. Instrum. Meth. A **586** (2008) 409-420.
[2] A. Castellina for the Pierre Auger Collaboration, UHECR 2018, EPJ Web Conf. **210** (2019) 06002.
[3] The Pierre Auger Collaboration, JINST **16** (2021) P04003.
[4] The Pierre Auger Collaboration, Nucl. Instrum. Meth. A **613** (2010) 29–31.
[5] The Pierre Auger Collaboration, JINST **16** (2021) T07008.
[6] A. Botti *et al.*, JINST **16** (2021) P07059.
[7] A. Botti for the Pierre Auger Collaboration, Proc. 37th Int. Cosmic Ray Conf. **PoS** (ICRC2021) 233.
[8] The Pierre Auger Collaboration, JINST **12** (2017) P03002.

The Pierre Auger Collaboration

A. Abdul Halim[13], P. Abreu[72], M. Aglietta[54,52], I. Allekotte[1], K. Almeida Cheminant[70], A. Almela[7,12], R. Aloisio[45,46], J. Alvarez-Muñiz[79], J. Ammerman Yebra[79], G.A. Anastasi[54,52], L. Anchordoqui[86], B. Andrada[7], S. Andringa[72], C. Aramo[50], P.R. Araújo Ferreira[42], E. Arnone[63,52], J. C. Arteaga Velázquez[67], H. Asorey[7], P. Assis[72], G. Avila[11], E. Avocone[57,46], A.M. Badescu[75], A. Bakalova[32], A. Balaceanu[73], F. Barbato[45,46], A. Bartz Mocellin[85], J.A. Bellido[13,69], C. Berat[36], M.E. Bertaina[63,52], G. Bhatta[70], M. Bianciotto[63,52], P.L. Biermann[h], V. Binet[5], K. Bismark[39,7], T. Bister[80,81], J. Biteau[37], J. Blazek[32], C. Bleve[36], J. Blümer[41], M. Boháčová[32], D. Boncioli[57,46], C. Bonifazi[8,26], L. Bonneau Arbeletche[21], N. Borodai[70], J. Brack[j], P.G. Brichetto Orchera[7], F.L. Briechle[42], A. Bueno[78], S. Buitink[15], M. Buscemi[47,61], M. Büsken[39,7], A. Bwembya[80,81], K.S. Caballero-Mora[66], S. Cabana-Freire[79], L. Caccianiga[59,49], I. Caracas[38], R. Caruso[58,47], A. Castellina[54,52], F. Catalani[18], G. Cataldi[48], L. Cazon[79], M. Cerda[10], A. Cermenati[45,46], J.A. Chinellato[21], J. Chudoba[32], L. Chytka[33], R.W. Clay[13], A.C. Cobos Cerutti[6], R. Colalillo[60,50], A. Coleman[90], M.R. Coluccia[48], R. Conceição[72], A. Condorelli[37], G. Consolati[49,55], M. Conte[56,48], F. Convenga[41], D. Correia dos Santos[28], P.J. Costa[72], C.E. Covault[84], M. Cristinziani[44], C.S. Cruz Sanchez[3], S. Dasso[4,2], K. Daumiller[41], B.R. Dawson[13], R.M. de Almeida[28], J. de Jesús[7,41], S.J. de Jong[80,81], J.R.T. de Mello Neto[26,27], I. De Mitri[45,46], J. de Oliveira[17], D. de Oliveira Franco[21], F. de Palma[56,48], V. de Souza[19], E. De Vito[56,48], A. Del Popolo[58,47], O. Deligny[34], N. Denner[32], L. Deval[41,7], A. di Matteo[52], M. Dobre[73], C. Dobrigkeit[21], J.C. D'Olivo[68], L.M. Domingues Mendes[72], J.C. dos Anjos, R.C. dos Anjos[25], J. Ebr[32], F. Ellwanger[41], M. Emam[80,81], R. Engel[39,41], I. Epicoco[56,48], M. Erdmann[42], A. Etchegoyen[7,12], C. Evoli[45,46], H. Falcke[80,82,81], J. Farmer[89], G. Farrar[88], A.C. Fauth[21], N. Fazzini[e], F. Feldbusch[40], F. Fenu[41,d], A. Fernandes[72], B. Fick[87], J.M. Figueira[7], A. Filipčič[77,76], T. Fitoussi[41], B. Flaggs[90], T. Fodran[80], T. Fujii[89,f], A. Fuster[7,12], C. Galea[80], C. Galelli[59,49], B. García[6], C. Gaudu[38], H. Gemmeke[40], F. Gesualdi[7,41], A. Gherghel-Lascu[73], P.L. Ghia[34], U. Giaccari[48], M. Giammarchi[49], J. Glombitza[42,g], F. Gobbi[10], F. Gollan[7], G. Golup[1], M. Gómez Berisso[1], P.F. Gómez Vitale[11], J.P. Gongora[11], J.M. González[1], N. González[7], I. Goos[1], D. Góra[70], A. Gorgi[54,52], M. Gottowik[79], T.D. Grubb[13], F. Guarino[60,50], G.P. Guedes[22], E. Guido[44], S. Hahn[39], P. Hamal[32], M.R. Hampel[7], P. Hansen[3], D. Harari[1], V.M. Harvey[13], A. Haungs[41], T. Hebbeker[42], C. Hojvat[e], J.R. Hörandel[80,81], P. Horvath[33], M. Hrabovský[33], T. Huege[41,15], A. Insolia[58,47], P.G. Isar[74], P. Janecek[32], J.A. Johnsen[85], J. Jurysek[32], A. Kääpä[38], K.H. Kampert[38], B. Keilhauer[41], A. Khakurdikar[80], V.V. Kizakke Covilakam[7,41], H.O. Klages[41], M. Kleifges[40], F. Knapp[39], N. Kunka[40], B.L. Lago[16], N. Langner[42], M.A. Leigui de Oliveira[24], Y Lema-Capeans[79], V. Lenok[39], A. Letessier-Selvon[35], I. Lhenry-Yvon[34], D. Lo Presti[58,47], L. Lopes[72], L. Lu[91], Q. Luce[39], J.P. Lundquist[76], A. Machado Payeras[21], M. Majercakova[32], D. Mandat[32], B.C. Manning[13], P. Mantsch[e], S. Marafico[34], F.M. Mariani[59,49], A.G. Mariazzi[3], I.C. Mariş[14], G. Marsella[61,47], D. Martello[56,48], S. Martinelli[41,7], O. Martínez Bravo[64], M.A. Martins[79], M. Mastrodicasa[57,46], H.J. Mathes[41], J. Matthews[a], G. Matthiae[62,51], E. Mayotte[85,38], S. Mayotte[85], P.O. Mazur[e], G. Medina-Tanco[68], J. Meinert[38], D. Melo[7], A. Menshikov[40], C. Merx[41], S. Michal[33], M.I. Micheletti[5], L. Miramonti[59,49], S. Mollerach[1], F. Montanet[36], L. Morejon[38], C. Morello[54,52], A.L. Müller[32], K. Mulrey[80,81], R. Mussa[52], M. Muzio[88], W.M. Namasaka[38], S. Negi[32], L. Nellen[68], K. Nguyen[87], G. Nicora[9], M. Niculescu-Oglinzanu[73], M. Niechciol[44], D. Nitz[87], D. Nosek[31], V. Novotny[31], L. Nožka[33], A Nucita[56,48], L.A. Núñez[30], C. Oliveira[19], M. Palatka[32], J. Pallotta[9], S. Panja[32], G. Parente[79], T. Paulsen[38], J. Pawlowsky[38], M. Pech[32], J. Pękala[70], R. Pelayo[65], L.A.S. Pereira[23], E.E. Pereira Martins[39,7], J. Perez Armand[20], C. Pérez Bertolli[7,41], L. Perrone[56,48], S. Petrera[45,46], C. Petrucci[57,46], T. Pierog[41], M. Pimenta[72], M. Platino[7], B. Pont[80], M. Pothast[81,80], M. Pourmohammad Shahvar[61,47], P. Privitera[89], M. Prouza[32], A. Puyleart[87], S. Querchfeld[38], J. Rautenberg[38], D. Ravignani[7], M. Reininghaus[39], J. Ridky[32], F. Riehn[79], M. Risse[44], V. Rizi[57,46], W. Rodrigues de Carvalho[80], E. Rodriguez[7,41], J. Rodriguez Rojo[11], M.J. Roncoroni[7], S. Rossoni[43], M. Roth[41], E. Roulet[1], A.C. Rovero[4], P. Ruehl[44], A. Saftoiu[73], M. Saharan[80], F. Salamida[57,46], H. Salazar[64], G. Salina[51], J.D. Sanabria Gomez[30], F. Sánchez[7], E.M. Santos[20], E. Santos[32],

F. Sarazin[85], R. Sarmento[72], R. Sato[11], P. Savina[91], C.M. Schäfer[41], V. Scherini[56,48], H. Schieler[41], M. Schimassek[34], M. Schimp[38], F. Schlüter[41], D. Schmidt[39], O. Scholten[15,i], H. Schoorlemmer[80,81], P. Schovánek[32], F.G. Schröder[90,41], J. Schulte[42], T. Schulz[41], S.J. Sciutto[3], M. Scornavacche[7,41], A. Segreto[53,47], S. Sehgal[38], S.U. Shivashankara[76], G. Sigl[43], G. Silli[7], O. Sima[73,b], F. Simon[40], R. Smau[73], R. Šmída[89], P. Sommers[k], J.F. Soriano[86], R. Squartini[10], M. Stadelmaier[32], D. Stanca[73], S. Stanič[76], J. Stasielak[70], P. Stassi[36], S. Strähnz[39], M. Straub[42], M. Suárez-Durán[14], T. Suomijärvi[37], A.D. Supanitsky[7], Z. Svozilikova[32], Z. Szadkowski[71], A. Tapia[29], C. Taricco[63,52], C. Timmermans[81,80], O. Tkachenko[41], P. Tobiska[32], C.J. Todero Peixoto[18], B. Tomé[72], Z. Torrès[36], A. Travaini[10], P. Travnicek[32], C. Trimarelli[57,46], M. Tueros[3], M. Unger[41], L. Vaclavek[33], M. Vacula[33], J.F. Valdés Galicia[68], L. Valore[60,50], E. Varela[64], A. Vásquez-Ramírez[30], D. Veberič[41], C. Ventura[27], I.D. Vergara Quispe[3], V. Verzi[51], J. Vicha[32], J. Vink[83], J. Vlastimil[32], S. Vorobiov[76], C. Watanabe[26], A.A. Watson[c], A. Weindl[41], L. Wiencke[85], H. Wilczyński[70], D. Wittkowski[38], B. Wundheiler[7], B. Yue[38], A. Yushkov[32], O. Zapparrata[14], E. Zas[79], D. Zavrtanik[76,77], M. Zavrtanik[77,76]

[1] Centro Atómico Bariloche and Instituto Balseiro (CNEA-UNCuyo-CONICET), San Carlos de Bariloche, Argentina
[2] Departamento de Física and Departamento de Ciencias de la Atmósfera y los Océanos, FCEyN, Universidad de Buenos Aires and CONICET, Buenos Aires, Argentina
[3] IFLP, Universidad Nacional de La Plata and CONICET, La Plata, Argentina
[4] Instituto de Astronomía y Física del Espacio (IAFE, CONICET-UBA), Buenos Aires, Argentina
[5] Instituto de Física de Rosario (IFIR) – CONICET/U.N.R. and Facultad de Ciencias Bioquímicas y Farmacéuticas U.N.R., Rosario, Argentina
[6] Instituto de Tecnologías en Detección y Astropartículas (CNEA, CONICET, UNSAM), and Universidad Tecnológica Nacional – Facultad Regional Mendoza (CONICET/CNEA), Mendoza, Argentina
[7] Instituto de Tecnologías en Detección y Astropartículas (CNEA, CONICET, UNSAM), Buenos Aires, Argentina
[8] International Center of Advanced Studies and Instituto de Ciencias Físicas, ECyT-UNSAM and CONICET, Campus Miguelete – San Martín, Buenos Aires, Argentina
[9] Laboratorio Atmósfera – Departamento de Investigaciones en Láseres y sus Aplicaciones – UNIDEF (CITEDEF-CONICET), Argentina
[10] Observatorio Pierre Auger, Malargüe, Argentina
[11] Observatorio Pierre Auger and Comisión Nacional de Energía Atómica, Malargüe, Argentina
[12] Universidad Tecnológica Nacional – Facultad Regional Buenos Aires, Buenos Aires, Argentina
[13] University of Adelaide, Adelaide, S.A., Australia
[14] Université Libre de Bruxelles (ULB), Brussels, Belgium
[15] Vrije Universiteit Brussels, Brussels, Belgium
[16] Centro Federal de Educação Tecnológica Celso Suckow da Fonseca, Petropolis, Brazil
[17] Instituto Federal de Educação, Ciência e Tecnologia do Rio de Janeiro (IFRJ), Brazil
[18] Universidade de São Paulo, Escola de Engenharia de Lorena, Lorena, SP, Brazil
[19] Universidade de São Paulo, Instituto de Física de São Carlos, São Carlos, SP, Brazil
[20] Universidade de São Paulo, Instituto de Física, São Paulo, SP, Brazil
[21] Universidade Estadual de Campinas, IFGW, Campinas, SP, Brazil
[22] Universidade Estadual de Feira de Santana, Feira de Santana, Brazil
[23] Universidade Federal de Campina Grande, Centro de Ciencias e Tecnologia, Campina Grande, Brazil
[24] Universidade Federal do ABC, Santo André, SP, Brazil
[25] Universidade Federal do Paraná, Setor Palotina, Palotina, Brazil
[26] Universidade Federal do Rio de Janeiro, Instituto de Física, Rio de Janeiro, RJ, Brazil
[27] Universidade Federal do Rio de Janeiro (UFRJ), Observatório do Valongo, Rio de Janeiro, RJ, Brazil
[28] Universidade Federal Fluminense, EEIMVR, Volta Redonda, RJ, Brazil
[29] Universidad de Medellín, Medellín, Colombia
[30] Universidad Industrial de Santander, Bucaramanga, Colombia

PoS(ICRC2023)267

[31] Charles University, Faculty of Mathematics and Physics, Institute of Particle and Nuclear Physics, Prague, Czech Republic
[32] Institute of Physics of the Czech Academy of Sciences, Prague, Czech Republic
[33] Palacky University, Olomouc, Czech Republic
[34] CNRS/IN2P3, IJCLab, Université Paris-Saclay, Orsay, France
[35] Laboratoire de Physique Nucléaire et de Hautes Energies (LPNHE), Sorbonne Université, Université de Paris, CNRS-IN2P3, Paris, France
[36] Univ. Grenoble Alpes, CNRS, Grenoble Institute of Engineering Univ. Grenoble Alpes, LPSC-IN2P3, 38000 Grenoble, France
[37] Université Paris-Saclay, CNRS/IN2P3, IJCLab, Orsay, France
[38] Bergische Universität Wuppertal, Department of Physics, Wuppertal, Germany
[39] Karlsruhe Institute of Technology (KIT), Institute for Experimental Particle Physics, Karlsruhe, Germany
[40] Karlsruhe Institute of Technology (KIT), Institut für Prozessdatenverarbeitung und Elektronik, Karlsruhe, Germany
[41] Karlsruhe Institute of Technology (KIT), Institute for Astroparticle Physics, Karlsruhe, Germany
[42] RWTH Aachen University, III. Physikalisches Institut A, Aachen, Germany
[43] Universität Hamburg, II. Institut für Theoretische Physik, Hamburg, Germany
[44] Universität Siegen, Department Physik – Experimentelle Teilchenphysik, Siegen, Germany
[45] Gran Sasso Science Institute, L'Aquila, Italy
[46] INFN Laboratori Nazionali del Gran Sasso, Assergi (L'Aquila), Italy
[47] INFN, Sezione di Catania, Catania, Italy
[48] INFN, Sezione di Lecce, Lecce, Italy
[49] INFN, Sezione di Milano, Milano, Italy
[50] INFN, Sezione di Napoli, Napoli, Italy
[51] INFN, Sezione di Roma "Tor Vergata", Roma, Italy
[52] INFN, Sezione di Torino, Torino, Italy
[53] Istituto di Astrofisica Spaziale e Fisica Cosmica di Palermo (INAF), Palermo, Italy
[54] Osservatorio Astrofisico di Torino (INAF), Torino, Italy
[55] Politecnico di Milano, Dipartimento di Scienze e Tecnologie Aerospaziali , Milano, Italy
[56] Università del Salento, Dipartimento di Matematica e Fisica "E. De Giorgi", Lecce, Italy
[57] Università dell'Aquila, Dipartimento di Scienze Fisiche e Chimiche, L'Aquila, Italy
[58] Università di Catania, Dipartimento di Fisica e Astronomia "Ettore Majorana", Catania, Italy
[59] Università di Milano, Dipartimento di Fisica, Milano, Italy
[60] Università di Napoli "Federico II", Dipartimento di Fisica "Ettore Pancini", Napoli, Italy
[61] Università di Palermo, Dipartimento di Fisica e Chimica "E. Segrè", Palermo, Italy
[62] Università di Roma "Tor Vergata", Dipartimento di Fisica, Roma, Italy
[63] Università Torino, Dipartimento di Fisica, Torino, Italy
[64] Benemérita Universidad Autónoma de Puebla, Puebla, México
[65] Unidad Profesional Interdisciplinaria en Ingeniería y Tecnologías Avanzadas del Instituto Politécnico Nacional (UPIITA-IPN), México, D.F., México
[66] Universidad Autónoma de Chiapas, Tuxtla Gutiérrez, Chiapas, México
[67] Universidad Michoacana de San Nicolás de Hidalgo, Morelia, Michoacán, México
[68] Universidad Nacional Autónoma de México, México, D.F., México
[69] Universidad Nacional de San Agustin de Arequipa, Facultad de Ciencias Naturales y Formales, Arequipa, Peru
[70] Institute of Nuclear Physics PAN, Krakow, Poland
[71] University of Łódź, Faculty of High-Energy Astrophysics,Łódź, Poland
[72] Laboratório de Instrumentação e Física Experimental de Partículas – LIP and Instituto Superior Técnico – IST, Universidade de Lisboa – UL, Lisboa, Portugal
[73] "Horia Hulubei" National Institute for Physics and Nuclear Engineering, Bucharest-Magurele, Romania
[74] Institute of Space Science, Bucharest-Magurele, Romania
[75] University Politehnica of Bucharest, Bucharest, Romania
[76] Center for Astrophysics and Cosmology (CAC), University of Nova Gorica, Nova Gorica, Slovenia
[77] Experimental Particle Physics Department, J. Stefan Institute, Ljubljana, Slovenia

PoS(ICRC2023)267

[78] Universidad de Granada and C.A.F.P.E., Granada, Spain
[79] Instituto Galego de Física de Altas Enerxías (IGFAE), Universidade de Santiago de Compostela, Santiago de Compostela, Spain
[80] IMAPP, Radboud University Nijmegen, Nijmegen, The Netherlands
[81] Nationaal Instituut voor Kernfysica en Hoge Energie Fysica (NIKHEF), Science Park, Amsterdam, The Netherlands
[82] Stichting Astronomisch Onderzoek in Nederland (ASTRON), Dwingeloo, The Netherlands
[83] Universiteit van Amsterdam, Faculty of Science, Amsterdam, The Netherlands
[84] Case Western Reserve University, Cleveland, OH, USA
[85] Colorado School of Mines, Golden, CO, USA
[86] Department of Physics and Astronomy, Lehman College, City University of New York, Bronx, NY, USA
[87] Michigan Technological University, Houghton, MI, USA
[88] New York University, New York, NY, USA
[89] University of Chicago, Enrico Fermi Institute, Chicago, IL, USA
[90] University of Delaware, Department of Physics and Astronomy, Bartol Research Institute, Newark, DE, USA
[91] University of Wisconsin-Madison, Department of Physics and WIPAC, Madison, WI, USA

—

[a] Louisiana State University, Baton Rouge, LA, USA
[b] also at University of Bucharest, Physics Department, Bucharest, Romania
[c] School of Physics and Astronomy, University of Leeds, Leeds, United Kingdom
[d] now at Agenzia Spaziale Italiana (ASI). Via del Politecnico 00133, Roma, Italy
[e] Fermi National Accelerator Laboratory, Fermilab, Batavia, IL, USA
[f] now at Graduate School of Science, Osaka Metropolitan University, Osaka, Japan
[g] now at ECAP, Erlangen, Germany
[h] Max-Planck-Institut für Radioastronomie, Bonn, Germany
[i] also at Kapteyn Institute, University of Groningen, Groningen, The Netherlands
[j] Colorado State University, Fort Collins, CO, USA
[k] Pennsylvania State University, University Park, PA, USA

Acknowledgments

The successful installation, commissioning, and operation of the Pierre Auger Observatory would not have been possible without the strong commitment and effort from the technical and administrative staff in Malargüe. We are very grateful to the following agencies and organizations for financial support:

Argentina – Comisión Nacional de Energía Atómica; Agencia Nacional de Promoción Científica y Tecnológica (ANPCyT); Consejo Nacional de Investigaciones Científicas y Técnicas (CONICET); Gobierno de la Provincia de Mendoza; Municipalidad de Malargüe; NDM Holdings and Valle Las Leñas; in gratitude for their continuing cooperation over land access; Australia – the Australian Research Council; Belgium – Fonds de la Recherche Scientifique (FNRS); Research Foundation Flanders (FWO); Brazil – Conselho Nacional de Desenvolvimento Científico e Tecnológico (CNPq); Financiadora de Estudos e Projetos (FINEP); Fundação de Amparo à Pesquisa do Estado de Rio de Janeiro (FAPERJ); São Paulo Research Foundation (FAPESP) Grants No. 2019/10151-2, No. 2010/07359-6 and No. 1999/05404-3; Ministério da Ciência, Tecnologia, Inovações e Comunicações (MCTIC); Czech Republic – Grant No. MSMT CR LTT18004, LM2015038, LM2018102, CZ.02.1.01/0.0/0.0/16_013/0001402, CZ.02.1.01/0.0/0.0/18_046/0016010 and CZ.02.1.01/0.0/0.0/17_049/0008422; France – Centre de Calcul IN2P3/CNRS; Centre National de la Recherche Scientifique (CNRS); Conseil Régional Ile-de-France; Département Physique Nucléaire et Corpusculaire (PNC-IN2P3/CNRS); Département Sciences de l'Univers (SDU-INSU/CNRS); Institut Lagrange de Paris (ILP) Grant No. LABEX ANR-10-LABX-63 within the Investissements d'Avenir Programme Grant No. ANR-11-IDEX-0004-02; Germany – Bundesministerium für Bildung und Forschung (BMBF); Deutsche Forschungsgemeinschaft (DFG); Finanzministerium Baden-Württemberg; Helmholtz Alliance for Astroparticle Physics (HAP); Helmholtz-Gemeinschaft Deutscher Forschungszentren (HGF); Ministerium für Kultur und Wissenschaft des Landes Nordrhein-Westfalen; Ministerium für Wissenschaft, Forschung und Kunst des Landes Baden-Württemberg; Italy – Istituto Nazionale di Fisica Nucleare (INFN); Istituto Nazionale di Astrofisica (INAF); Ministero dell'Istruzione, dell'Universitá e della Ricerca (MIUR); CETEMPS Center

of Excellence; Ministero degli Affari Esteri (MAE), ICSC Centro Nazionale di Ricerca in High Performance Computing, Big Data and Quantum Computing, funded by European Union NextGenerationEU, reference code CN_00000013; México – Consejo Nacional de Ciencia y Tecnología (CONACYT) No. 167733; Universidad Nacional Autónoma de México (UNAM); PAPIIT DGAPA-UNAM; The Netherlands – Ministry of Education, Culture and Science; Netherlands Organisation for Scientific Research (NWO); Dutch national e-infrastructure with the support of SURF Cooperative; Poland – Ministry of Education and Science, grants No. DIR/WK/2018/11 and 2022/WK/12; National Science Centre, grants No. 2016/22/M/ST9/00198, 2016/23/B/ST9/01635, 2020/39/B/ST9/01398, and 2022/45/B/ST9/02163; Portugal – Portuguese national funds and FEDER funds within Programa Operacional Factores de Competitividade through Fundação para a Ciência e a Tecnologia (COMPETE); Romania – Ministry of Research, Innovation and Digitization, CNCS-UEFISCDI, contract no. 30N/2023 under Romanian National Core Program LAPLAS VII, grant no. PN 23 21 01 02 and project number PN-III-P1-1.1-TE-2021-0924/TE57/2022, within PNCDI III; Slovenia – Slovenian Research Agency, grants P1-0031, P1-0385, I0-0033, N1-0111; Spain – Ministerio de Economía, Industria y Competitividad (FPA2017-85114-P and PID2019-104676GB-C32), Xunta de Galicia (ED431C 2017/07), Junta de Andalucía (SOMM17/6104/UGR, P18-FR-4314) Feder Funds, RENATA Red Nacional Temática de Astropartículas (FPA2015-68783-REDT) and María de Maeztu Unit of Excellence (MDM-2016-0692); USA – Department of Energy, Contracts No. DE-AC02-07CH11359, No. DE-FR02-04ER41300, No. DE-FG02-99ER41107 and No. DE-SC0011689; National Science Foundation, Grant No. 0450696; The Grainger Foundation; Marie Curie-IRSES/EPLANET; European Particle Physics Latin American Network; and UNESCO.